

# Verifiable Benchmarking of Long-Horizon Spatial Biology

Evaluating whether AI agents can recover complex scientific conclusions from raw spatial biology data

Ian Diks<sup>1\*</sup>, Harihara Muralidharan<sup>1\*</sup>, Tim Proctor<sup>1</sup>, Kenny Workman<sup>1\*</sup>

<sup>1</sup>LatchBio, San Francisco, CA, USA

\*Equal contribution

Correspondence: kenny@latch.bio

## ABSTRACT

AI agents are increasingly useful for biological data analysis, but existing benchmarks mostly test broad biological knowledge, executable workflows, or localized analysis steps rather than end-to-end scientific reasoning over spatial measurements. We introduce SpatialBench-Long, a benchmark for long-horizon spatial biology in which agents must recover biological claims from raw or near-raw data and calibrated experimental context without prescribed methods. SpatialBench-Long contains 24 evaluations across primary pancreatic ductal adenocarcinoma (PDAC), engineered glioblastoma organoids and in vivo tumors, Cas9 lineage-traced lung adenocarcinoma, and mouse optic nerve aging/intervention systems, spanning CosMx, Visium, Xenium, multiplexed error-robust fluorescence in situ hybridization (MER-FISH), single-cell RNA sequencing (scRNA-seq), Slide-seq, Slide-tags, histology, and lineage-recording data. Candidate claims are hardened through reproduction, independent scientist review, and trajectory inspection. Final answers are graded deterministically over controlled vocabularies and symbols with companion rubrics capturing progress through key analysis chokepoints. Across the SpatialBench-Long benchmark, three model-harness pairs tie at 8/72 runs (11.1%): Gemini 3.5 Flash / Pi terminal coding harness, GPT-5.5 / Pi, and GPT-5.5 / OpenAI Codex. SpatialBench-Long tests whether agents can move beyond executing procedural analysis to deriving accurate scientific conclusions from complex spatial measurements.

arXiv:submit/7642990 [cs.AI] 27 May 2026

# Topline Benchmark Performance

We ran the benchmark across frontier model families and agent harnesses. Pi denotes the Pi terminal coding harness. Passing requires exact recovery of the graded structured answer for an evaluation attempt. Present systems show low but nonzero success rates: Gemini 3.5 Flash / Pi, GPT-5.5 / Pi, and GPT-5.5 / OpenAI Codex each pass 8/72 runs.

Pass rate by model-harness pair

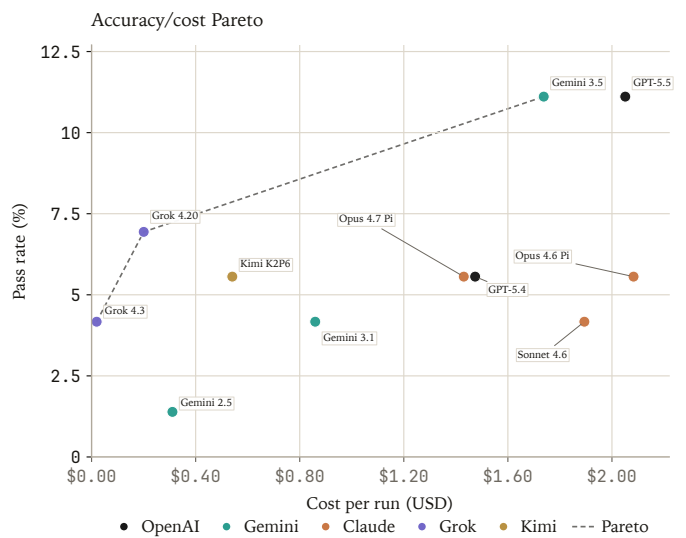
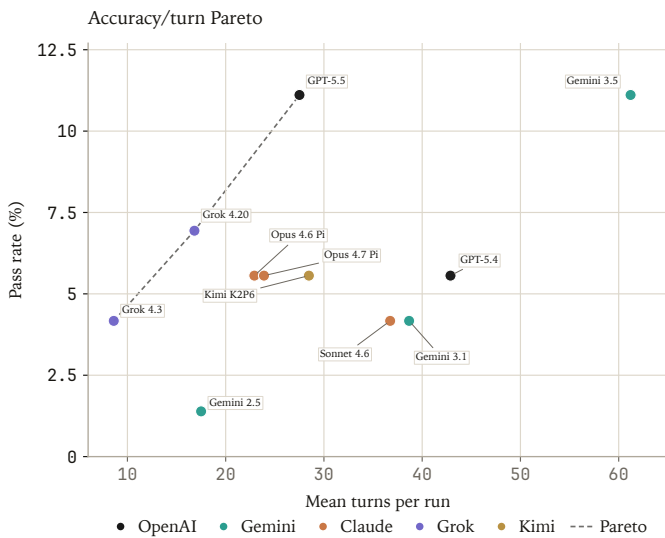
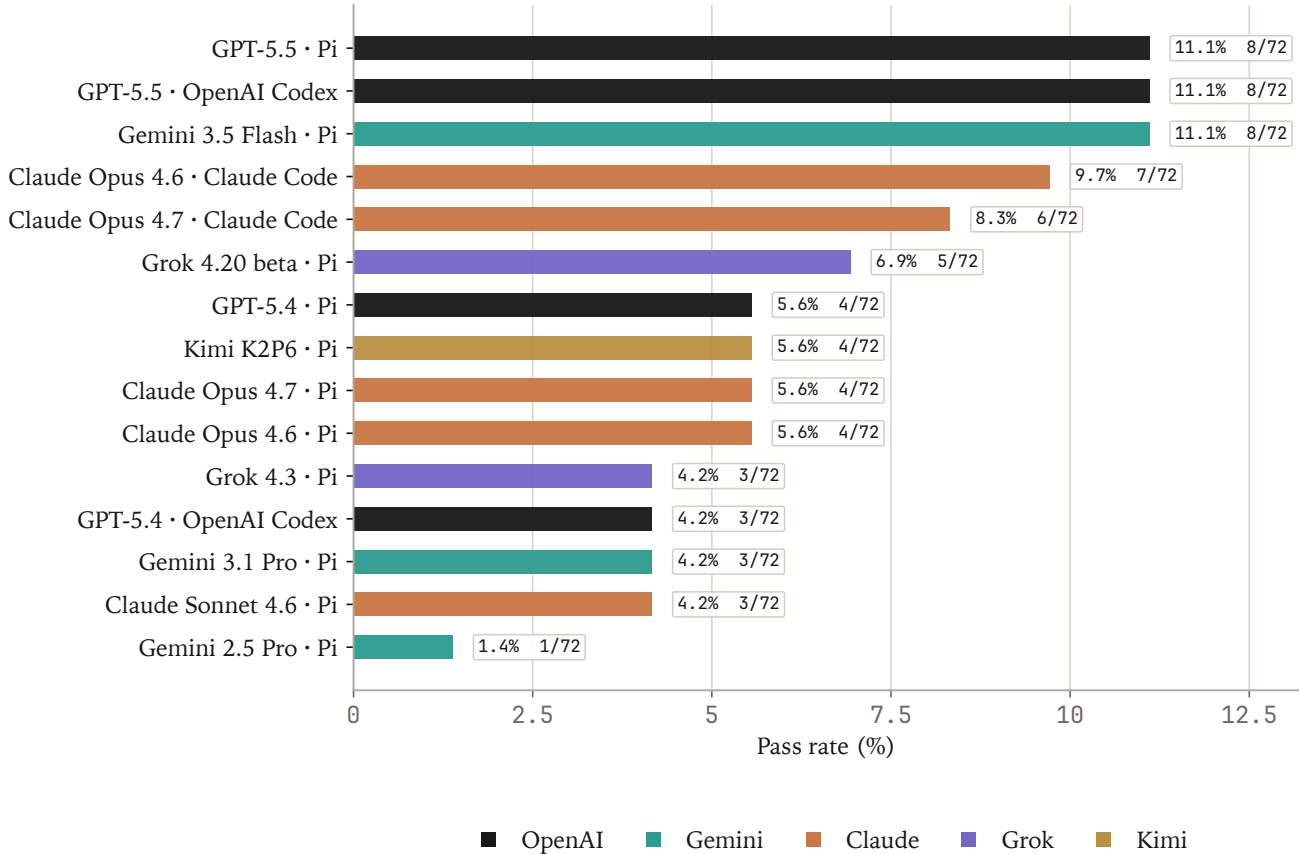


**Figure 1: Topline benchmark performance.** Top: pass rate by model-harness pair across the complete benchmark set. Bottom left: pass rate against mean agent turns. Bottom right: pass rate against mean cost. Confidence intervals and evaluation-level replicate statistics are reported in Table 2

# Introduction

Scientists use spatial biology data in open-ended research contexts to construct new knowledge about living systems. Raw measurements do not directly encode scientific conclusions. They must be processed through multi-step workflows, integrated with other assays, interpreted against experimental design, and contextualized with both prior literature and the original goal of the study [1, 2, 3].

AI agents are beginning to show utility in biological data analysis, but they still struggle to contextualize analysis decisions within scientific goals, use assay-specific knowledge accurately, and distinguish conclusions supported by the provided data from plausible claims drawn from prior literature [17, 18, 19].

Prior benchmarks focus on complementary aspects of scientific work: broad biology reasoning benchmarks emphasize coverage, bioinformatics-agent benchmarks emphasize executable workflows, and spatial-analysis benchmarks emphasize deterministic grading of localized analysis steps [24, 25, 26, 27, 28, 19, 17, 18]. However, no current benchmark

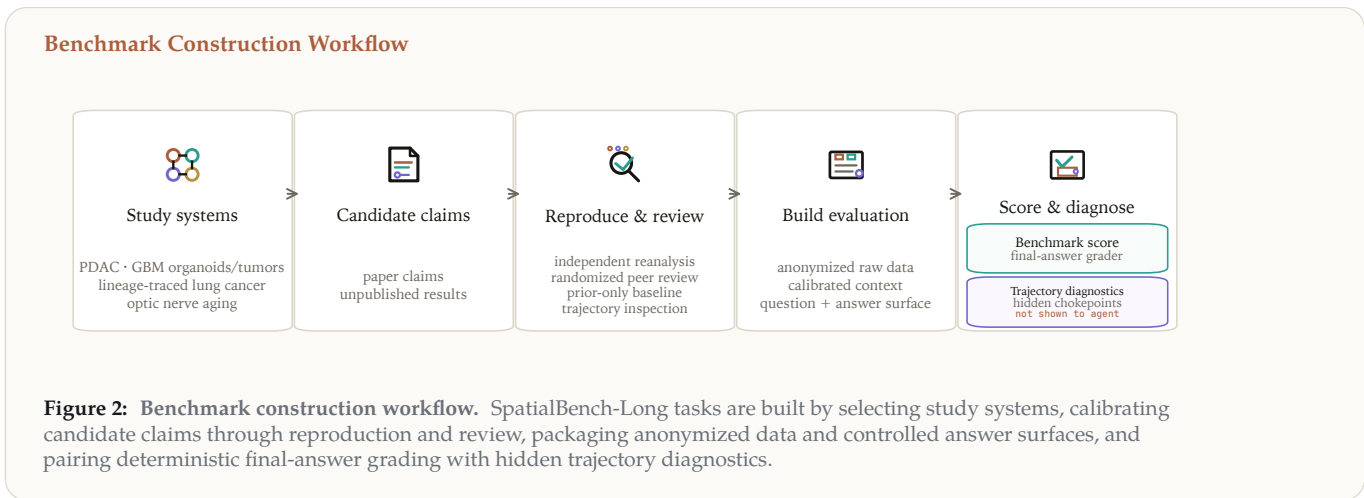
investigates whether an agent can undertake the end-to-end work of recovering a specific scientific conclusion from raw spatial measurements, calibrated context, and many possible analysis paths.

Raw spatial data rarely admits a single universal ground truth. The same measurements and experimental context can support multiple valid scientific conclusions, and unanticipated but true claims can be drawn from a dataset. Published claims can also fail to reproduce cleanly under unbiased reanalysis [29, 30, 31, 32].

SpatialBench-Long evaluates whether agents can recover specified scientific conclusions from raw spatial biology data and experimental context. Each task provides a scientific question, raw or near-raw data, relevant assay context, and a verifiable solution. The benchmark reports binary pass/fail grading on final scientific conclusions and pairs verifiable scores with rubric-based trajectory diagnostics that identify progress through key analysis chokepoints [17, 18]. In the 24-evaluation benchmark run set, the top three model-harness pairs each pass 8/72 runs, motivating diagnostic analyses that distinguish total failure from partial scientific progress.

# Benchmark Design

Agents are evaluated on end scientific conclusions from 24 evaluations spanning four study systems: primary pancreatic ductal adenocarcinoma (PDAC), engineered glioblastoma (GBM) organoids and in vivo tumors, Cas9 lineage-traced lung adenocarcinoma, and mouse optic nerve aging and intervention [4, 5, 6, 11]. Across the benchmark, evaluations draw on modalities including spatial transcriptomics, histology, single-cell references, and lineage-recording data.



This organization reflects the structure of real spatial biology projects. Solving these tasks requires cross-assay reasoning, experimental-design awareness, and command of complex spatial biology workflows: tissue segmentation, cell-neighborhood and niche analysis, spatial differential expression, reference-based cell-type mapping, and histology–transcriptome alignment [3, 12, 13, 14, 15, 16].

Each evaluation includes experimental context, raw data, and

a scientific question. Task information is calibrated to approximate what a scientist would know when beginning the analysis, balancing over-specification against ambiguity. Task descriptions and raw-data labels are scrubbed for identifying information about the original study. In many cases, the task tests an unpublished result or is structured so that memorized literature alone is unlikely to solve it [26, 27].

Identifying durable ground truths is especially challenging

in long-horizon biological benchmarking. Naive paper-claim reproduction is brittle because the same data may support multiple valid conclusions, and some published claims do not reproduce cleanly under unbiased reanalysis [29, 30, 31, 33]. We therefore use paper claims as sources for candidate evaluations rather than as automatic ground truth. Candidate tasks are refined through independent reproduction, randomized expert review, and inspection of trajectories from multiple model families. Many candidate claims were excluded because they did not reproduce robustly from the provided data.

Grading uses deterministic functions over structured final answers. Rather than grading isolated numerical outputs from individual statistical operations, SpatialBench-Long grades recovery of scientific conclusions expressed through controlled biological vocabularies, ordered relationships or direction labels [17, 18, 26].

Manual trajectory inspection is a first-class part of benchmark construction. Model trajectories and randomized expert attempts are used to stress-test task context, target answers, and grading assumptions. Evaluation authors maintain reproduction notes and rubrics describing known decision chokepoints. These notes aid manual trajectory interpretation and provide a record for future benchmark updates, especially as stronger models may solve tasks through unanticipated but valid analysis paths that challenge current grading assumptions [19].

## Verifiable grading paired with rubric diagnostics

Benchmark scores use verifiable pass/fail grading on final outcomes. In practice, failures to construct a verifiable grader usually indicated that a candidate task lacked a reproducible target claim, that the provided context was miscalibrated, or

that the answer surface had not yet been constrained enough for deterministic evaluation [17, 18, 26].

However, final-answer grading provides sparse diagnostic signal for long-horizon tasks. A model can fail the benchmark while solving many subproblems correctly, and deterministic grading necessarily penalizes answers outside the pre-specified target surface, including some valid claims not anticipated by the benchmark authors [20, 19].

We considered verifiable grading of intermediate steps, but found that specifying those steps risked leaking information about the intended solution path or biasing the agent’s analysis trajectory. We therefore use rubric-based trajectory judging as a companion diagnostic rather than as the benchmark score. These rubric scores are prompt-sensitive and reflect the authors’ current model of the task, but they provide higher-resolution information about partial progress and help identify cases where grading assumptions should be revisited [20, 19].

Evaluation authors define chokepoints after independent reproduction, peer review, and inspection of trajectories from multiple model families. Chokepoints are analysis decisions or biological constraints expected to remain stable across plausible solution paths. Examples include choosing the correct biological comparison, identifying the relevant assay or spatial compartment, performing a necessary sanity check or avoiding a known trap.

Chokepoint rubrics are then used by large language model (LLM) judges to score model trajectories. We report their correlation with verifiable pass/fail outcomes and their consistency across replicates and model families, treating rubric scores as diagnostic evidence rather than replacement benchmark scores [19, 21, 22, 23].

# Motivating Example: Can an Agent Reconstruct A Primary Pro-Metastatic Cancer Niche

## Lineage-tracing Chokepoint Schematic

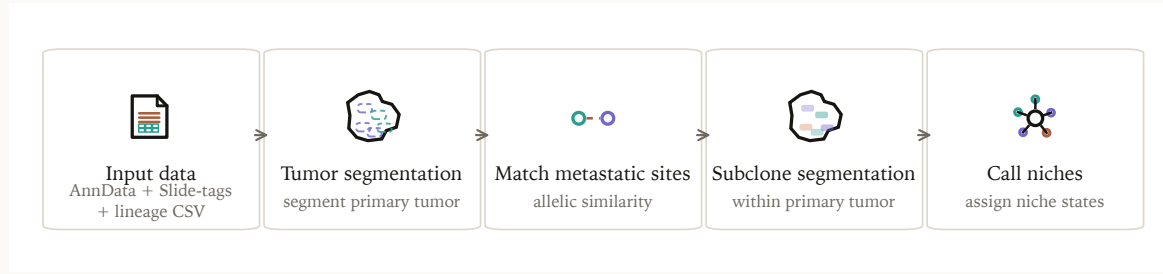


**Figure 3: Primary pro-metastatic niche reconstruction.** The lineage-tracing task compresses a long spatial workflow into a verifiable structure. Agents must stage spatial and lineage inputs, segment candidate primary tumor regions, match metastatic references by allelic distance, define met-like subregions within the primary tumor, and call enriched or depleted niche programs while avoiding plausible generic metastasis signals.

One evaluation begins with a compact biological question: which expression programs characterize the primary-tumor regions most related to distant metastases? The source study combines spatial transcriptomics with Cas9 lineage tracing in a *Kras*;p53 lung adenocarcinoma model [6, 7]. Cre induction both initiates tumor formation and activates lineage recording, producing heritable target-site edits that mark tumor subclones [8]. Slide-seq and Slide-tags then measure spatial transcriptional state together with lineage-target transcripts, making it possible to ask how clonal history and local microenvironment vary across primary and metastatic lesions [9, 10, 6].

The agent is given anonymized spatial expression arrays of primary tumors and metastatic lesions, lineage allele tables, distant metastatic references, and a controlled vocabulary of candidate programs. It must reconstruct primary-tumor niches most lineage-similar to distant metastases compared to non-metastatic regions of the same primary tumor.

The evaluation authors identified a series of chokepoints. The agent must first stage the spatial and lineage data together instead of relying only on gene expression data; segment candidate primary tumor regions without falling outside shape and count uncharacteristic of lung cancer; use allelic distance to

connect metastatic references back to primary regions instead of relying expression similarity; define a spatially coherent metastatic subregion within the primary tumor; and finally call niche programs consistent across multiple layers of the primary tumor and separating the primary pro-metastatic niche from distant-site remodeling or generic metastasis signatures.

The deterministic grader scores only the final primary tumor niches with the correct directions. The accepted enriched programs include epithelial-to-mesenchymal transition (EMT), hypoxia, immunosuppressive macrophage, scavenger macrophage, and fibrotic programs, while alveolar differentiation and gastric/endoderm programs are depleted. Nearby alternatives such as collagen deposition, myogenesis, blood-vessel programs, and generic metastasis signatures are biologically plausible but rejected or ambiguous for this specific primary-niche claim after analyzing multiple analysis paths.

This example shows why rubric scores are useful even when the benchmark score is binary. A model can trip up in the final stages of the evaluation, such as only considering a single primary tumor layer and picking a distractor niche with an incorrect local direction while making considerable correct progress.

# Evaluation Inventory

SpatialBench-Long is organized around studies instead of independent datasets. Each study contributes a cluster of evaluations that asks different scientific questions of the same experimental context while varying the relevant assays and tasks.

Across the four studies, the benchmark currently contains 24 long-horizon evaluations. Primary PDAC contributes the largest cluster, with tasks over CosMx, Visium data from formalin-fixed paraffin-embedded (FFPE) tissue, paired CosMx/Visium evidence, and histology. Engineered glioblastoma (GBM) organoid tasks combine Xenium, matched single-cell RNA sequencing (scRNA-seq), and patient GBM single-cell references. Lung adenocarcinoma tasks pair Slide-seq and Slide-tags spatial measurements with Cas9 lineage recording. Optic nerve tasks use multiplexed error-robust fluorescence in situ hybridization (MERFISH) single-cell spatial transcriptomics in aging and intervention settings. H&E denotes hematoxylin and eosin staining; CAF, TME, and TLS denote cancer-associated fibroblast, tumor microenvironment, and tertiary lymphoid structure, respectively.

Study/system	Evals	Assays / data types	Main task themes
Primary PDAC	11	CosMx, Visium FFPE, paired CosMx+Visium, H&E/trichrome	Classical-basal axis, CAF/immune/TME shifts, hypoxia, TLS, perineural niches, collagen and histology integration
Glioblastoma organoids / in vivo tumors	4	Xenium, matched scRNA-seq, patient GBM single-cell RNA reference	Organoid niche disruption, proximity changes, in vivo tumor architecture, malignant cell-state composition
Lung adenocarcinoma lineage tracing	5	Slide-seq, Slide-tags, Cas9 lineage recording	Metastasis-origin matching, metastatic-site programs, tumor fitness, pro-metastatic primary niches
Mouse optic nerve aging/intervention	4	MERFISH single-cell spatial transcriptomics	Aging niche shifts, chemokine source attribution, spatial colocalization, condition-anonymized disruption

**Table 1: Evaluation inventory.** SpatialBench-Long groups evaluations by study while varying the claim, workflow, data types, and task objectives.

Across these evaluations, assay coverage includes CosMx-only tasks, Visium and Visium-plus-histology tasks, mixed CosMx/Visium tasks, Xenium and scRNA-seq reference tasks, MERFISH tasks, and Slide-seq/Slide-tags/Cas9-lineage tasks. The task set emphasizes spatial niche and architecture reasoning, cross-platform reconciliation, tumor-state and microenvironment interpretation. The complete benchmark reports 15 model-harness pairs and 72 runs per pair across the 24 evaluations, for 1,080 trajectories.

# Results

## Verifiable grading stratifies frontier models with low pass rates

Across 15 model-harness pairs and 1,080 trajectories, Gemini 3.5 Flash / Pi, GPT-5.5 / Pi, and GPT-5.5 / OpenAI Codex each passed 8/72 attempts (11.11%; Wilson 95% confidence interval (CI), 5.74–20.42), with Claude Opus 4.6 / Claude

Code close behind at 7/72 attempts (9.72%). Most remaining model-harness pairs passed 3–5/72 attempts, while Gemini 2.5 Pro / Pi passed 1/72. Success was therefore low across all systems and not cleanly separated among the leading models. Evaluation-level replicate statistics help distinguish occasional success from clearer task recovery: even among the leading systems, passing at least one replicate was observed for only 4–5 of 24 evaluations, and majority-replicate passing for only 2 of 24 (Figure 4; Table 2).

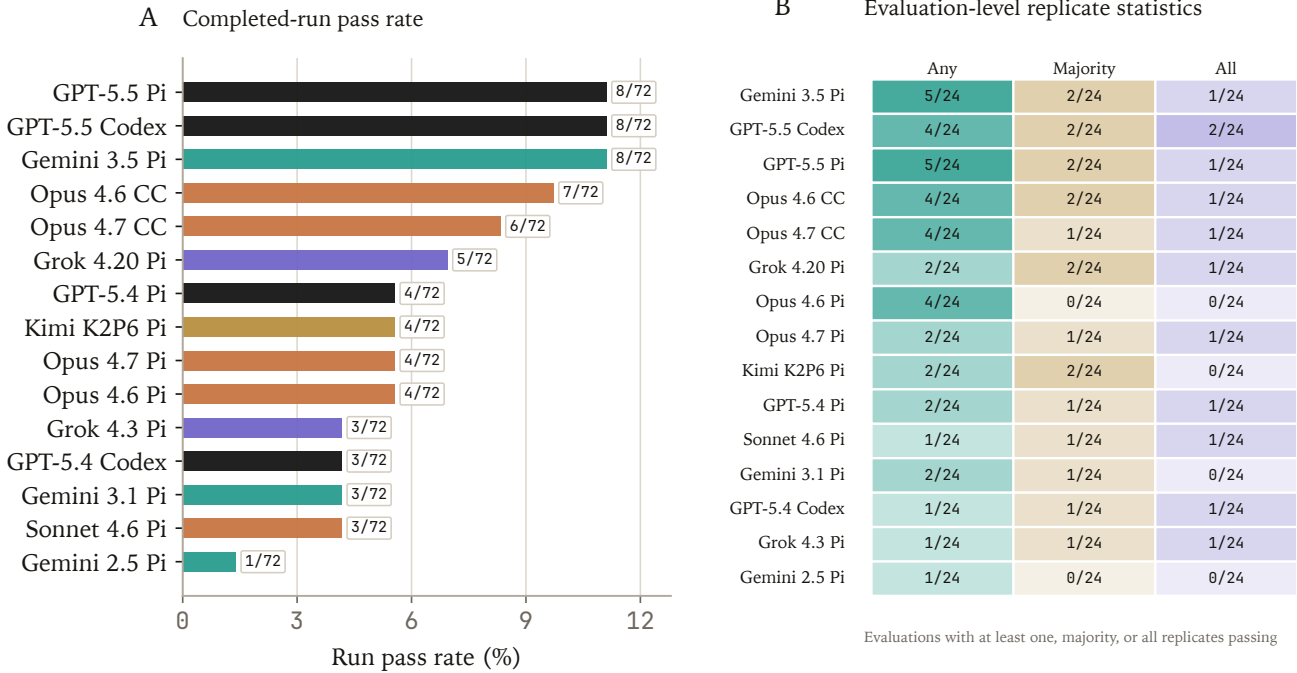


**Figure 4: Sparse endpoint success across model-harness pairs.** Deterministic final-answer performance across 24 SpatialBench-Long evaluations. The left panel reports passing trajectories out of 72 attempts per model-harness pair. The right panel reports evaluation-level replicate statistics: the number of evaluations with at least one passing replicate, a majority of passing replicates, or all replicates passing. Wilson confidence intervals are omitted from the figure and reported in Table 2.

Model / harness	Pass runs	Pass %	Wilson 95% CI	Any	Majority	All	Cost	Turns
Gemini 3.5 Flash / Pi	8/72	11.11	5.74–20.42	5/24	2/24	1/24	\$1.7378	61.21
GPT-5.5 / OpenAI Codex	8/72	11.11	5.74–20.42	4/24	2/24	2/24	–	–
GPT-5.5 / Pi	8/72	11.11	5.74–20.42	5/24	2/24	1/24	\$2.0512	27.51
Claude Opus 4.6 / Claude Code	7/72	9.72	4.79–18.74	4/24	2/24	1/24	–	–
Claude Opus 4.7 / Claude Code	6/72	8.33	3.88–17.01	4/24	1/24	1/24	–	–
Grok 4.20 beta / Pi	5/72	6.94	3.00–15.25	2/24	2/24	1/24	\$0.2004	16.82
Claude Opus 4.6 / Pi	4/72	5.56	2.18–13.43	4/24	0/24	0/24	\$2.0830	22.92
Claude Opus 4.7 / Pi	4/72	5.56	2.18–13.43	2/24	1/24	1/24	\$1.4305	23.90
Kimi K2P6 / Pi	4/72	5.56	2.18–13.43	2/24	2/24	0/24	\$0.5409	28.47
GPT-5.4 / Pi	4/72	5.56	2.18–13.43	2/24	1/24	1/24	\$1.4742	42.88
Claude Sonnet 4.6 / Pi	3/72	4.17	1.43–11.55	1/24	1/24	1/24	\$1.8940	36.74
Gemini 3.1 Pro / Pi	3/72	4.17	1.43–11.55	2/24	1/24	0/24	\$0.8596	38.67
GPT-5.4 / OpenAI Codex	3/72	4.17	1.43–11.55	1/24	1/24	1/24	–	–
Grok 4.3 / Pi	3/72	4.17	1.43–11.55	1/24	1/24	1/24	\$0.0195	8.61
Gemini 2.5 Pro / Pi	1/72	1.39	0.25–7.46	1/24	0/24	0/24	\$0.3108	17.50

**Table 2: Deterministic final-answer performance.** Model-harness results across the 24-evaluation SpatialBench-Long benchmark. Pass runs and pass percentage report endpoint success over 72 attempts per model-harness pair. Wilson intervals summarize run-level binomial uncertainty and do not account for evaluation-level clustering; evaluation-level replicate statistics are reported separately in the Any, Majority, and All columns. Cost and turn-count summaries are shown where comparable metadata are available; code-harness result JSONs lacking these fields are shown with dashes.

## Rubric Judges Are Reproducible and Associated with Endpoint Success

Rubric judges are used as companion diagnostics to measure partial progress and interpret model behavior against sparse final-answer binary grading. We scored 792 trajectories with four judges, yielding 3,145 valid scores out of 3,168 expected scores (99.27%). Of these trajectories, 770 had valid scores from all four judges and 791 had valid scores from at least three.

Rubric scores were associated but not perfectly correlated with endpoint success. Among trajectories with four valid judge scores, endpoint-passing runs had higher mean rubric scores than endpoint-failing runs (72.2%, bootstrap 95% CI 62.1–80.9, vs. 45.8%, 44.1–47.5). The four-judge rubric mean showed a modest association with deterministic pass/fail status (Pearson

$r = 0.24$ , bootstrap 95% CI 0.16–0.33; Spearman  $\rho = 0.24$ ; receiver operating characteristic area under the curve (ROC AUC) = 0.79, bootstrap 95% CI 0.70–0.88; Figure 5).

Judge-to-judge reproducibility was high. Mean pairwise judge correlation was 0.93, the minimum pairwise correlation was 0.91, and the mean absolute pairwise score difference was 6.2 percentage points. Same-trajectory cross-judge variability was smaller than variation across independent attempts on the same evaluation: judge standard deviation (SD) averaged 5.3 points per trajectory, while replicate SD averaged 8.7 points across eval-by-source-model groups with at least two trajectories (Figure 5).

These results support rubric scores as reproducible diagnostic annotations: they are informative but imperfect predictors of curated endpoint success, not substitutes for verifiable final-answer grading.

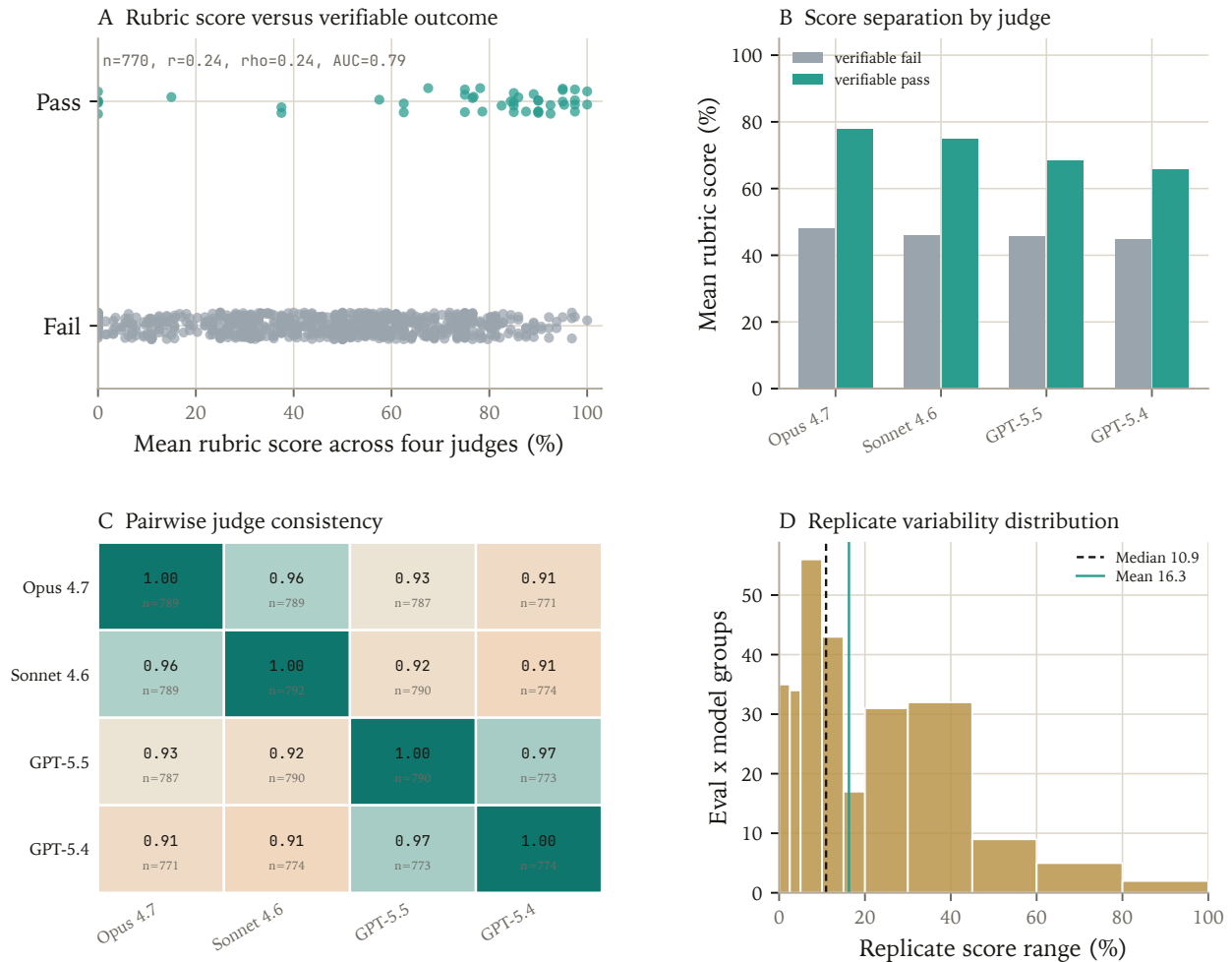


**Figure 5: Rubric diagnostics are reproducible and endpoint-associated.** Rubric-judge analysis across the 792-trajectory judge matrix. Panel A compares mean four-judge rubric score with deterministic pass/fail outcomes for trajectories with all four valid judge scores. Panel B shows the same pass/fail separation by judge. Panel C reports pairwise judge-score correlations on matched trajectories. Panel D shows rubric-score variation across independent attempts from the same source model and evaluation. Rubric scores are used as diagnostic trajectory annotations, not as benchmark pass/fail scores.

## Rubric Scores Are Useful but Do Not Replace Verifiable Grading

Strict endpoint grading makes reward sparse. In the 792-trajectory judge matrix, only 47 trajectories passed the deterministic grader (5.9%). Replicate pass rates were more informative but still zero for most trajectories, with nonzero scores for 275/714 trajectories (38.5%). By contrast, mean rubric score was nonzero for 725/770 trajectories (94.2%), indicating that rubric judging supplies much denser trajectory-level signal than endpoint grading (Figure 6).

We were interested in exploring the utility of rubric grading for intermediate reward and asked if denser signal was partially aligned with endpoint quality. Mean four-judge rubric score correlated with replicate pass rate score at Pearson  $r = 0.361$  (eval-cluster bootstrap 95% CI 0.074–0.573;  $n = 692$ ) and Spearman  $\rho = 0.338$  (0.085–0.552).

To check that this association was not driven only by differences in evaluation difficulty, we repeated the analysis after centering scores within each evaluation. The correlation remained similar ( $r = 0.340$ , 0.149–0.510), indicating that higher-scored trajectories were more likely to succeed even among attempts on the same evaluation.

The relationship between endpoint grading and rubrics was uneven. Verifiable scores were enriched in the highest rubric decile, where the pass rate reached 34.2%, but pass rates were noisy and nonmonotonic across the middle deciles. Thus, very high rubric scores identify trajectories enriched for endpoint success, while small or moderate rubric-score differences should not be interpreted as calibrated differences in scientific quality.

Rubric scores also varied systematically by source model. After controlling for evaluation identity, normalized verifiable score, and pass/fail status, mean residual rubric scores still differed substantially across source models and model families. Source-model residuals ranged from -26.8 to +11.6 percentage points, while source-family residuals ranged from -20.9 to +11.2 points. Raw rubric scores therefore appear to reflect not only endpoint success, but also trajectory style, model family, and possible judge-style effects (Figure 6).

Together, these analyses support rubric scores as promising auxiliary tools, not substitutes for verifiable endpoint grading. High rubric scores enrich for endpoint success, but moderate score differences are not calibrated measures of scientific correctness. Stronger validation requires expert trajectory audits to decide whether deviations are valid alternate analyses, rubric over-credit, or ordinary model errors.

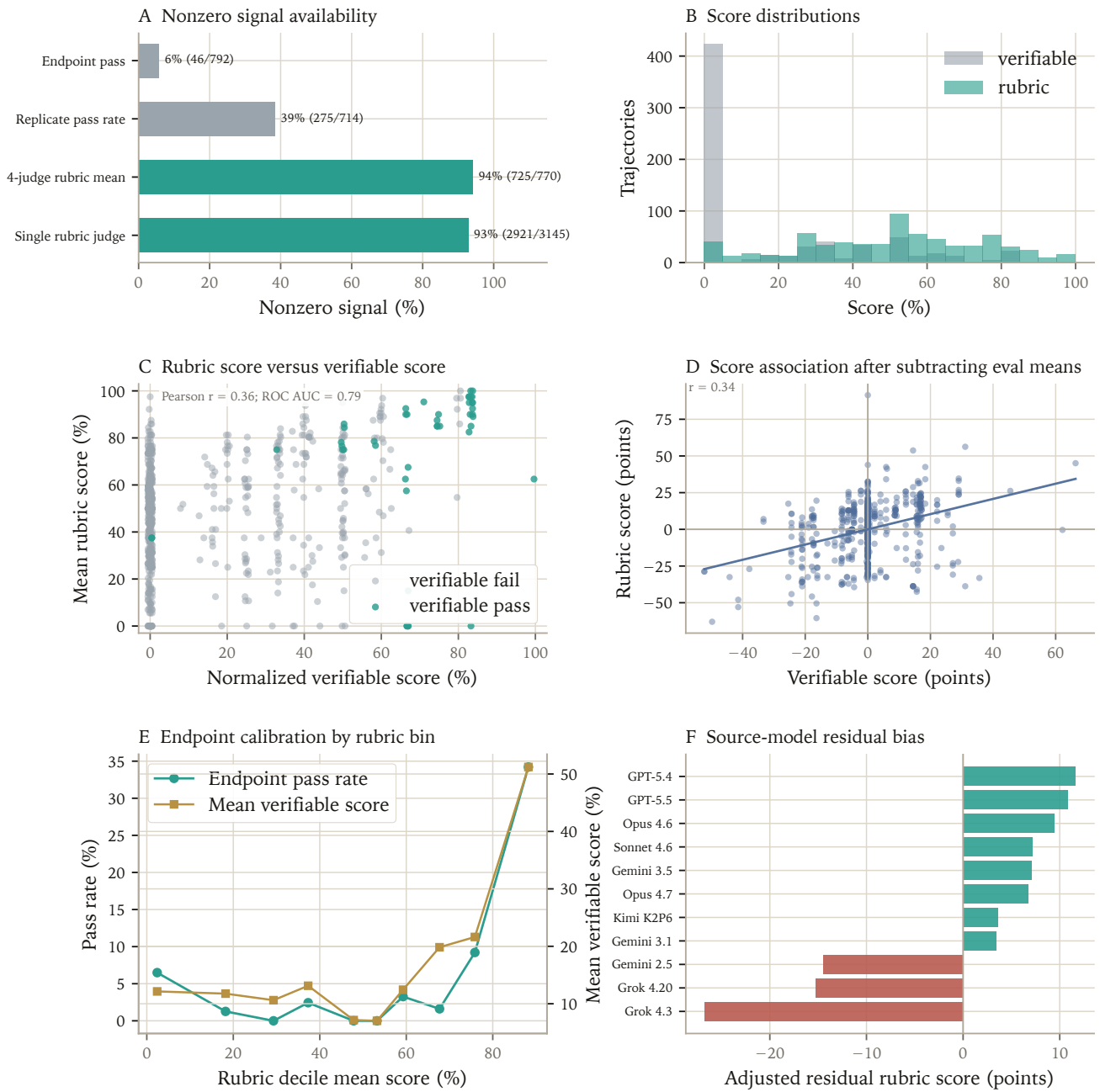


**Figure 6: Rubric scores provide dense but imperfect auxiliary signal.** Panel A compares nonzero rates for deterministic endpoint passes, replicate-pass rate, mean rubric score, and single-judge rubric score. Panel B compares the corresponding score distributions. Panel C shows the relationship between mean rubric score and replicate pass rate for the corresponding evaluation-by-source-model group. Panel D shows the same relationship after subtracting each evaluation’s mean from both scores. Panel E reports endpoint pass rate by rubric-score decile. Panel F reports source-model residual rubric variation after controlling for evaluation identity and normalized verifiable score, and pass/fail status. Rubric scores are denser than endpoint grading, but are not calibrated substitutes for verifiable pass/fail outcomes.

## Rubric Scores Vary by Source Model and Trajectory Style

We next stratified rubric scores by the source agent model whose trajectory was being judged to see if rubric patterns are consistent across judges. Mean four-judge rubric scores were highest for OpenAI and Anthropic trajectories. GPT-5.4 and GPT-5.5 both averaged about 63%, while Claude Opus 4.6, Claude Opus 4.7, and Claude Sonnet 4.6 averaged about 60%, 56%, and 56%, respectively. Gemini 3.5 Flash had one of the strongest verifiable profiles but a lower mean rubric score (46.5%), suggesting brittleness in either our rubrics or

ground truths. Kimi, Grok 4.20, Gemini 2.5 Pro, and Grok 4.3 had lower mean rubric scores, ranging from 38.3% to 23.4% (Figure 7).

These source-model patterns were consistent across judges. All four judges preserved the same broad ordering across source models, while differing modestly in absolute score level. Mean four-judge rubric score also correlated with replicate-level endpoint signal (Pearson  $r = 0.36$ ; Spearman  $\rho = 0.34$ ;  $n = 692$ ), but within-model correlations were descriptive rather than inferential because endpoint passes were sparse and each model family produced a different mix of failure modes.

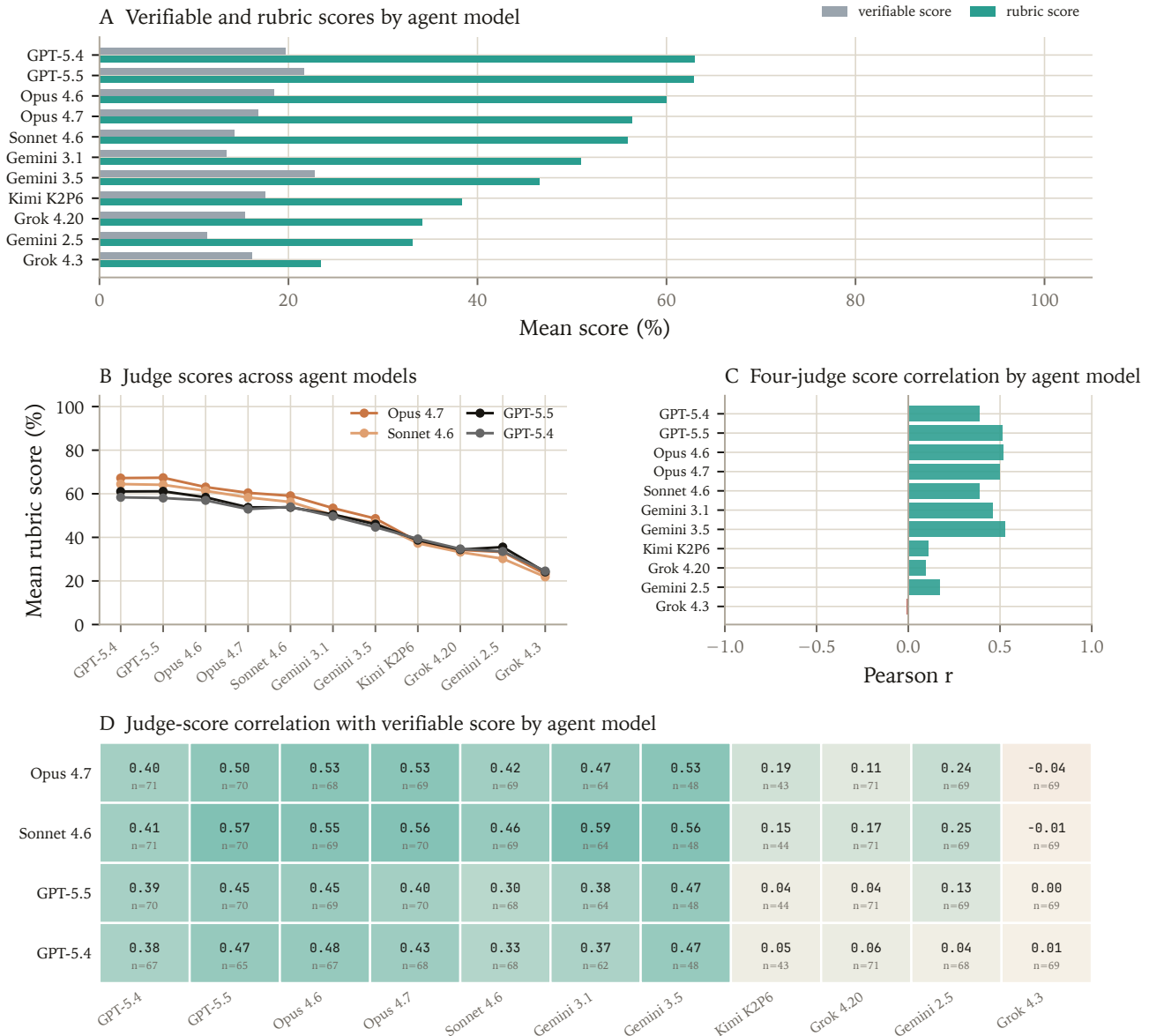


**Figure 7: Rubric scores vary by source agent model.** Panel A compares replicate-level endpoint signal with mean four-judge rubric score across source agent models. Panel B shows judge-specific rubric scores by source model. Panel C reports within-model correlations between mean four-judge rubric score and replicate-level endpoint signal. Panel D shows the judge-by-agent-model correlation matrix.

## Model Behavior Descriptions

Manual trajectory review identified seven recurring behavior groups. Two groups with high rubric scores involved failures after doing most of the work and collecting the requisite context. In final-decision failures, agents selected the wrong final target. In partial-credit answers, agents returned some accepted components but lost credit through omissions, aliases, controlled-vocabulary mismatch, or distractor selection.

The remaining modes reflected deeper analysis failures. Twelve trajectories missed important metadata or sanity-check context, most clearly in adult/aged optic-nerve tasks where agents consistently missed intentionally swapped metadata labels. Ten used the wrong grouping variable, especially in lin-

age tasks where agents used expression intensity, whole-allele overlap, or generic primary-versus-metastasis contrasts instead of lineage-aware comparisons. Six used an inappropriate spatial method by clustering expression rather than neighborhoods, pooling coordinates across sections, or annotating phantom cell types. Six relied on prior biology or vocabulary hints instead of analyzing the data. Three failed through local computation or data-wrangling issues.

Failure modes also differed by source model family. OpenAI and Anthropic trajectories had the highest mean rubric score and most often failed at the final decision after substantial analysis. Gemini failures often involved the wrong grouping variable, threshold rules, or data wrangling. xAI and Kimi failures skewed toward more shallow analysis.

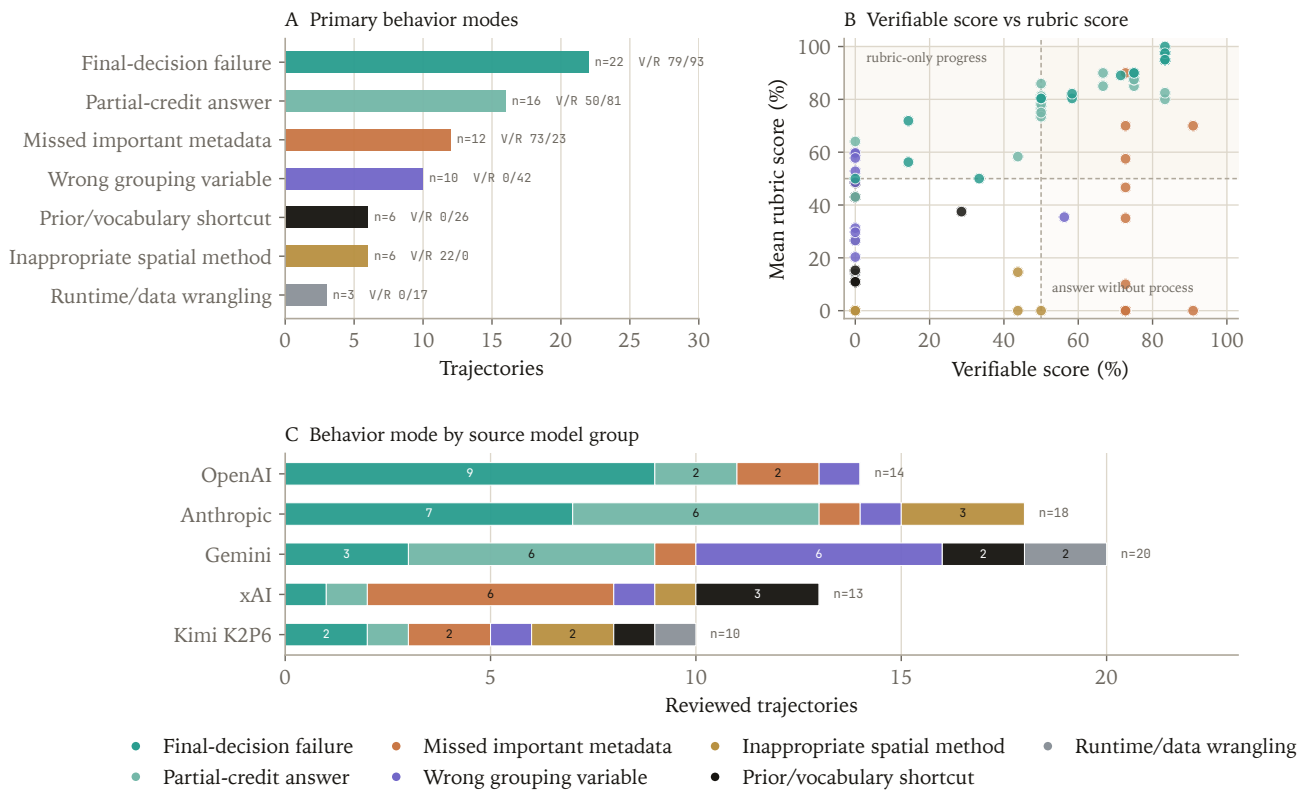


**Figure 8: Trajectory behavior modes.** Panel A summarizes the primary behavior mode assigned to each of the 75 reviewed calibration trajectories. Inline labels report the count and median verifiable/rubric score percentages for each group. Panel B compares normalized verifiable score with mean rubric score across the same reviewed trajectories, showing how rubric diagnostics separate shallow shortcuts, missed metadata, partial-credit answers, and final-decision failures that can look similar under final-answer grading alone. Panel C stratifies the same behavior modes by source model group.

## Discussion

---

SpatialBench-Long evaluates whether AI agents can recover specific scientific claims from raw spatial biology measurements and calibrated experimental context. The benchmark preserves the open-ended structure of real analysis: agents are not given prescribed methods, but must choose comparisons, process assay-specific data, integrate spatial and molecular evidence, and return a constrained scientific conclusion. This design makes evaluation more difficult than procedural benchmarks, but exposes whether agents can coordinate many local analysis decisions into a correct biological claim.

Current frontier agents show low but nonzero capability on this benchmark. The leading model-harness pairs each passed at least one replicate on only 4–5 of 24 evaluations, and achieved majority-replicate success on only 2 of 24 evaluations, despite each passing 8 of 72 total attempts. Success was therefore sparse at both the run level and the evaluation level. Rubric diagnostics and trajectory review suggest that compounding local analysis errors, rather than absence of general biological knowledge, prevent reliable long-horizon scientific reasoning.

Before models can reliably reason about disease mechanisms, drug response, or other deep results in biology, they must become procedurally competent at concrete molecular measurements. In spatial biology, that means understanding the properties and constraints of individual kits, machines, panels, tissue types, coordinate systems, segmentation outputs, normalization regimes, and experimental designs. Just as coding agents had to become reliable at local software tasks before attempting larger systems, biology agents will likely progress from assay-specific analysis competence to emergent biological reasoning, and only later to synthesis across modalities, translational context, and realistic ambiguity. Benchmarks such as SpatialBench-Long are intended to make that progression measurable.

## Methods

---

### Benchmark assembly

Benchmark construction is described in the Benchmark Design section. Briefly, we assembled 24 evaluations from four study systems spanning primary PDAC, engineered glioblastoma organoids and in vivo tumors, Cas9 lineage-traced lung adenocarcinoma, and mouse optic nerve aging/intervention. Candidate evaluations were retained when the target claim could be reproduced from the provided data, expressed through a constrained answer surface, and graded deterministically. Tasks were excluded when the claim was not reproducible, the context was insufficient or overdetermined, or the answer surface could not be made stable. Each retained evaluation includes a prompt, raw or near-raw data, controlled vocabulary, output schema, hidden grader, and task-specific rubric. Dataset

labels and study context were anonymized or scrubbed where needed to reduce memorization and literature-lookup shortcuts.

### Agent runs

We evaluated 15 model-harness pairs across Pi (the Pi terminal coding harness), OpenAI Codex, and Claude Code harnesses. Each pair was run on all 24 evaluations with three independent replicates, yielding 72 runs per pair and 1,080 final trajectories. Runs used the packaged evaluation inputs, hidden graders, a shared execution environment, tool access for file inspection and analysis, and fixed resource/time limits. For each run we recorded the final answer, grader output, trajectory, logs, duration, and available cost/turn metadata. Failed, timed-out, malformed, or incomplete runs were retained in denominators and counted as nonpassing unless the deterministic grader emitted a passing result. Cost and turn analyses are restricted to the Pi harness, where those fields were consistently logged.

### Endpoint grading

The primary benchmark score is deterministic endpoint grading of the final structured answer. Graders parse the submitted output, compare fields against task-specific schemas and controlled vocabularies, and compute run-level pass/fail plus available component scores. Malformed, missing, or unparsable answers are counted as failures. We aggregate endpoint results as run-level pass rates and as evaluation-level replicate passing counts: the number of evaluations for which a model-harness pair passes any replicate, a majority of replicates, or all replicates.

### Rubric judging

For diagnostic analysis, each evaluation has a chokepoint rubric describing expected scientific progress through key analysis decisions and known traps. Rubric scores are not benchmark scores. We scored the Pi-harness trajectory matrix with four judge models: Opus 4.7, Sonnet 4.6, GPT-5.5, and GPT-5.4, yielding 3,168 expected judge scores over 792 trajectories. Judges saw the trajectory, task context, and rubric, and returned structured criterion scores. Scores were normalized by rubric maximum and averaged across valid judges. Invalid or missing judge outputs were excluded from judge-specific analyses; matched-judge analyses use trajectories with the required valid scores.

### Statistical analysis

Run-level pass rates use Wilson binomial confidence intervals. Rubric analyses use bootstrap confidence intervals, clustered by evaluation when trajectories from the same task are compared. Associations between rubric and endpoint scores are reported with Pearson and Spearman correlations; pass/fail dis-

crimination is reported with ROC AUC. For within-evaluation analyses, rubric and verifiable scores were centered by evaluation to ask whether rubric scores rank trajectories within the same task. Residual rubric-bias analyses control for evaluation identity, normalized verifiable score, and pass/fail status.

## Manual trajectory review

We manually reviewed 75 trajectories selected to cover passes, ordinary failures, high-rubric failures, low-rubric passes, high judge-disagreement cases, and high replicate-variation groups. Reviewers assigned qualitative behavior modes: final-decision failure, partial-credit answer, missed important metadata, wrong grouping variable, inappropriate spatial method, prior/vocabulary shortcut, or runtime/data-wrangling breakdown. Reviewers also flagged possible grader, rubric, or ground-truth issues separately from ordinary model failures.

## Data availability

Results files and a subset of evaluations and trajectories are available at <https://github.com/latchbio/spatialbench-long>.

## References

- [1] Moses, L. & Pachter, L. Museum of spatial transcriptomics. *Nature Methods* **19**, 534–546 (2022). <https://doi.org/10.1038/s41592-022-01409-2>.
- [2] Williams, C. G., Lee, H. J., Asatsuma, T., Vento-Tormo, R. & Haque, A. An introduction to spatial transcriptomics for biomedical research. *Genome Medicine* **14**, 68 (2022). <https://doi.org/10.1186/s13073-022-01075-1>.
- [3] Dries, R., Chen, J., Del Rossi, N., Khan, M. M., Sistig, A. & Yuan, G. C. Advances in spatial transcriptomic data analysis. *Genome Research* **31**, 1706–1718 (2021). <https://doi.org/10.1101/gr.275224.121>.
- [4] Lyubetskaya, A., Rabe, B., Kavran, A., Bai, Y. et al. *In situ* multi-modal characterization of pancreatic cancer reveals tumor cell identity as a defining factor of the surrounding microenvironment. *Cell Reports* **45**, 116827 (2026). <https://doi.org/10.1016/j.celrep.2025.116827>.
- [5] Ishahak, M., Han, R. H., Annamalai, D., Woodiwiss, T., McCornack, C., Cleary, R. T., DeSouza, P. A., Qu, X., Dahiya, S., Kim, A. H. & Millman, J. R. Genetically engineered brain organoids recapitulate spatial and developmental states of glioblastoma progression. *Advanced Science* **12**, 2410110 (2025). <https://doi.org/10.1002/adv.202410110>.
- [6] Jones, M. G., Sun, D., Min, K. H. J., Colgan, W. N., Wang, H., Torok, T., Cardoso, E. C., Tian, L., Weir, J. A., Chen, V. Z., Koblan, L. W., Yost, K. E., Mathey-Andrews, N., D'Souza, E., Russell, A. J. C., Stickels, R. R., Balderrama, K. S., Rideout, W. M., Dai, M., Marrero, G., Kumar, V., Saqi, A., Chen, F., Weissman, J. S., Yosef, N. & Yang, D. Spatiotemporal lineage tracing reveals the dynamic spatial architecture of tumor growth and metastasis. *bioRxiv* (2024). <https://doi.org/10.1101/2024.10.21.619529>.
- [7] Yang, D., Jones, M. G., Naranjo, S., Rideout, W. M., Min, K. H. J., Ho, R., Wu, W., Replogle, J. M., Page, J. L., Quinn, J. J., Horns, F., Qiu, X., Chen, M. Z., Freed-Pastor, W. A., McGinnis, C. S., Patterson, D. M., Gartner, Z. J., Chow, E. D., Bivona, T. G., Chan, M. M., Yosef, N., Jacks, T. & Weissman, J. S. Lineage tracing reveals the phylogenetics, plasticity, and paths of tumor evolution. *Cell* **185**, 1905–1923.e25 (2022). <https://doi.org/10.1016/j.cell.2022.04.015>.
- [8] DuPage, M., Dooley, A. L. & Jacks, T. Conditional mouse lung cancer models using adenoviral or lentiviral delivery of Cre recombinase. *Nature Protocols* **4**, 1064–1072 (2009). <https://doi.org/10.1038/nprot.2009.95>.
- [9] Rodrigues, S. G., Stickels, R. R., Goeva, A., Martin, C. A., Murray, E., Vanderburg, C. R., Welch, J., Chen, L. M., Chen, F. & Macosko, E. Z. Slide-seq: A scalable technology for measuring genome-wide expression at high spatial resolution. *Science* **363**, 1463–1467 (2019). <https://doi.org/10.1126/science.aaw1219>.
- [10] Russell, A. J. C., Weir, J. A., Nadaf, N. M., Shabet, M., Kumar, V., Kambhampati, S., Raichur, R., Marrero, G. J., Liu, S., Balderrama, K. S., Vanderburg, C. R., Shanmugam, V., Tian, L., Iorgulescu, J. B., Yoon, C. H., Wu, C. J., Macosko, E. Z. & Chen, F. Slide-tags enables single-nucleus barcoding for multimodal spatial genomics. *Nature* **625**, 101–109 (2024). <https://doi.org/10.1038/s41586-023-06837-4>.
- [11] Groh, J., Feng, R., Yuan, X., Liu, L., Klein, D. et al. Microglia activation orchestrates CXCL10-mediated CD8+ T cell recruitment to promote aging-related white matter degeneration. *Nature Neuroscience* **28**, 1160–1173 (2025). <https://doi.org/10.1038/s41593-025-01955-w>.
- [12] Singhal, V., Chou, N., Lee, J., Yue, Y., Liu, J., Chock, W. K., Lin, L., Chang, Y.-C., Teo, E. M. L., Aow, J., Lee, H. K., Chen, K. H. & Prabhakar, S. BANKSY unifies cell typing and tissue domain segmentation for scalable spatial omics data analysis. *Nature Genetics* **56**, 431–441 (2024). <https://doi.org/10.1038/s41588-024-01664-3>.
- [13] Varrone, M., Tavernari, D., Santamaria-Martinez, A., Walsh, L. A. et al. CellCharter reveals spatial cell niches associated with tissue remodeling and cell plasticity. *Nature Genetics* **56**, 74–84 (2024). <https://doi.org/10.1038/s41588-023-01588-4>.

- [14] Qin, F., Luo, X., Lu, Q., Cai, B., Xiao, F. & Cai, G. Spatial pattern and differential expression analysis with spatial transcriptomic data. *Nucleic Acids Research* **52**, e101 (2024). <https://doi.org/10.1093/nar/gkae962>.
- [15] Kleshchevnikov, V., Shmatko, A., Dann, E., Aivazidis, A., King, H. W., Li, T., Elmentaite, R., Lomakin, A., Kedlian, V., Gayoso, A., Jain, M. S., Park, J. S., Ramona, L., Tuck, E., Arutyunyan, A., Vento-Tormo, R., Gerstung, M., James, L., Stegle, O. & Bayraktar, O. A. Cell2location maps fine-grained cell types in spatial transcriptomics. *Nature Biotechnology* **40**, 661–671 (2022). <https://doi.org/10.1038/s41587-021-01139-4>.
- [16] Biancalani, T., Scalia, G., Buffoni, L., Avasthi, R., Lu, Z., Sanger, A., Tokcan, N., Vanderburg, C. R., Segerstolpe, A., Zhang, M., Avraham-Davidi, I. & Regev, A. Deep learning and alignment of spatially resolved single-cell transcriptomes with Tangram. *Nature Methods* **18**, 1352–1362 (2021). <https://doi.org/10.1038/s41592-021-01264-7>.
- [17] Workman, K., Yang, Z., Muralidharan, H. & Le, H. SpatialBench: Can agents analyze real-world spatial biology data? *arXiv* arXiv:2512.21907 (2025). <https://doi.org/10.48550/arXiv.2512.21907>.
- [18] Workman, K., Yang, Z., Muralidharan, H., Abdulali, A. & Le, H. scBench: Evaluating AI agents on single-cell RNA-seq analysis. *arXiv* arXiv:2602.09063 (2026). <https://doi.org/10.48550/arXiv.2602.09063>.
- [19] Qu, Y., Lu, Y., Tu, X., Zhang, S., She, T., Shaw, A. G., Shih, J.-H., Zhao, B. et al. BiomniBench: Process-level evaluation of LLM agents for real-world biomedical research. *bioRxiv* (2026). <https://doi.org/10.64898/2026.05.12.724604>.
- [20] Lightman, H., Kosaraju, V., Burda, Y., Edwards, H., Baker, B., Lee, T., Leike, J., Schulman, J., Sutskever, I. & Cobbe, K. Let’s verify step by step. *arXiv* arXiv:2305.20050 (2023). <https://doi.org/10.48550/arXiv.2305.20050>.
- [21] Zheng, L., Chiang, W.-L., Sheng, Y., Zhuang, S., Wu, Z., Zhuang, Y., Lin, Z., Li, Z., Li, D., Xing, E. P., Zhang, H., Gonzalez, J. E. & Stoica, I. Judging LLM-as-a-judge with MT-Bench and Chatbot Arena. *arXiv* arXiv:2306.05685 (2023). <https://doi.org/10.48550/arXiv.2306.05685>.
- [22] Wang, P., Li, L., Chen, L., Cai, Z., Zhu, D., Lin, B., Cao, Y., Kong, L., Liu, Q., Liu, T. & Sui, Z. Large language models are not fair evaluators. In *Proceedings of the 62nd Annual Meeting of the Association for Computational Linguistics (Volume 1: Long Papers)*, 9440–9450 (2024). <https://doi.org/10.18653/v1/2024.acl-long.511>.
- [23] Liu, Y., Iter, D., Xu, Y., Wang, S., Xu, R. & Zhu, C. G-Eval: NLG evaluation using GPT-4 with better human alignment. In *Proceedings of the 2023 Conference on Empirical Methods in Natural Language Processing*, 2511–2522 (2023). <https://doi.org/10.18653/v1/2023.emnlp-main.153>.
- [24] Laurent, J. M., Janizek, J. D., Ruzo, M., Hinks, M. M., Hammerling, M. J., Narayanan, S., Ponnampati, M., White, A. D. & Rodrigues, S. G. LAB-Bench: Measuring capabilities of language models for biology research. *arXiv* arXiv:2407.10362 (2024). <https://doi.org/10.48550/arXiv.2407.10362>.
- [25] Mitchener, L., Laurent, J. M., Andonian, A., Tenmann, B., Narayanan, S., Wellawatte, G. P., White, A., Sani, L. & Rodrigues, S. G. BixBench: a comprehensive benchmark for LLM-based agents in computational biology. *arXiv* arXiv:2503.00096 (2025). <https://doi.org/10.48550/arXiv.2503.00096>.
- [26] Nair, S., Gunsalus, L., Orcutt-Jahns, B., Rossen, J., Lal, A., De Donno, C., Celik, M. H., Fletez-Brant, K., Xie, X., Corrada Bravo, H. & Eraslan, G. Agentic systems are adept at solving well-scoped, verifiable problems in computational biology. *bioRxiv* (2026). <https://doi.org/10.64898/2026.04.06.716850>.
- [27] Li, J. & Ho, A. GeneBench: Assessing AI agents for multi-stage inference problems in genomics and quantitative biology. *bioRxiv* (2026). <https://doi.org/10.64898/2026.04.22.720113>.
- [28] Anthropic. Evaluating Claude’s bioinformatics research capabilities with BioMysteryBench. *Anthropic Research* (2026). [anthropic.com/research/BioMysteryBench](https://anthropic.com/research/BioMysteryBench).
- [29] Ioannidis, J. P. A. Why most published research findings are false. *PLOS Medicine* **2**, e124 (2005). <https://doi.org/10.1371/journal.pmed.0020124>.
- [30] Prinz, F., Schlange, T. & Asadullah, K. Believe it or not: how much can we rely on published data on potential drug targets? *Nature Reviews Drug Discovery* **10**, 712 (2011). <https://doi.org/10.1038/nrd3439-c1>.
- [31] Begley, C. G. & Ellis, L. M. Raise standards for pre-clinical cancer research. *Nature* **483**, 531–533 (2012). <https://doi.org/10.1038/483531a>.
- [32] Errington, T. M., Denis, A., Perfito, N., Iorns, E. & Nosek, B. A. Reproducibility in Cancer Biology: Challenges for assessing replicability in preclinical cancer biology. *eLife* **10**, e67995 (2021). <https://doi.org/10.7554/eLife.67995>.
- [33] Errington, T. M., Mathur, M., Soderberg, C. K., Denis, A., Perfito, N., Iorns, E. & Nosek, B. A. Investigating the replicability of preclinical cancer biology. *eLife* **10**, e71601 (2021). <https://doi.org/10.7554/eLife.71601>.